Application of sentinel 2 to evaluate colored dissolved organic matter algorithms for inland water bodies in Jordan

Nidal M. Hussein [1], Mohammed N. Assaf [2,*] and Sohib S. Abohussein [3]

[1] Department of Civil Engineering, University of Petra, Amman – Jordan, ORCID:0000-0002-4188-7694, 201911339@uopstd.edu.jo;
[2] School of Natural Resources Engineering and Management, German Jordanian University, Amman, Jordan, ORCID: 0000-0002-4003-8690 ;
[3] Department of Civil Engineering, University of Petra, Amman –Jordan,
** Corresponding authors: nidal.hussein@uop.edu.jo ; 201911339@uopstd.edu.jo ; m.assaf@gju.edu.jo; Tel.:00962798893942.*

Abstract: The purpose of this article is to investigate the possibility of employing Multispectral Imager's (MSI) on Sentinel 2 to identify the colored dissolved organic matter (CDOM) in inland water. CDOM can be defined as an essential indicator of water quality as it has a key role in biogeochemical processing. This study held in three important Jordanian dams. Mujib, Wadi Al Arab, and lastly King Talal Dam. From these three dams, sixty water samples were taken fairly. The prediction models were validated using the remaining samples after the models were calibrated using forty samples. The predictive models were tested using the remaining samples .The results show that the sentinel 2 blue to green band (B2/B3) has provided the best CDOM retrieval algorithm with an accuracy coefficient of determination R^2= 0.8155, root-mean-squared error RMSE= 1.754 m^{-1}.The study showed that Sentinel 2 data might be used to determine CDOM in a variety of inland water body quality ranges, meaning that remote sensing can be a valuable tool for inland water quality monitoring. This study contains empirical data that can be utilized as a starting point for further research that includes more sites and circumstances.

Keywords: colored dissolved organic matter; remote sensing; Sentinel-2; Jordan dams

1. Introduction

Jordan is a relatively small country with limited natural resources. Jordan is categorized between arid and semi-arid countries [1]. According to recent statistics and reports, Jordan is the 3rd country in the world that suffers from freshwater storage [1-4]. Jordan water demand is around 900 MCM/yr; 75 % of it arises in the Jordan River Basin. Jordan's total dam capacity, including the desert dams, is projected to be 350 MCM. In the north and middle Jordan valleys, seven dams have been built, with a combined storage capacity of 270 MCM. Arab, Ziglab, King Talal, Karameh, Shueib, Kafrein, and Al Wehdah Dams are among them. In addition, three dams have been built in the southern Ghors: Wala, Mujib, and Tanner, with a total live storage of 30 MCM [2].

Jordan Inland water is considered a vital and primary water supply for drinking and irrigation [5]. The rivers, dams, and reservoirs are the most common examples of surface water, and they have significant significance for the environment's most valuable components (VECs). In addition, the dams play an essential role in providing good conditions for species, hydrological, climate-control, carbon-cycle, and nutrient-cycle processes [1].

Inland waters can be broadly described as the principal source of carbon delivery and transfer from ecosystems to aquatic environments [6]. Studies have shown that Inland water releases approximately 1.8 gigatons of Carbon dioxide to the atmosphere and transfer an equal amount of carbon to ocean waters [7]. This flow is higher than previously predicted, with dissolved organic carbon (DOC) from terrestrial ecosystems accounting for more than half of it [8]. As a result, riverine systems (streams and rivers) control a large portion of DOC export from terrestrial to aquatic ecosystems and the geographical and temporal variability of freshwater DOC in drainage watersheds [9]. The principal interaction regions are shallow coastal and estuarine environments to transfer carbon from terrestrial to the aquatic ecosystem.

Colored dissolved organic matter (CDOM) is the optically measurable component of dissolved organic matter in water, which can also be defined as chromophoric dissolved matter [10-14].

The CDOM peak absorption is found in the blue wavelength region and diminishing to around zero in the red region [15]. Several investigations have detected that COD concentrations are highly corrected to CDOM levels in both inland water and costal [16, 17]. Therefore, estimating CDOM absorption through remote sensing techniques will provide a better understanding of carbon cycling.

The term "satellite remote detection techniques" refers to a method for determining geophysical boundaries using electromagnetic radiation reflected or created by the earth [18]. Because of the optical properties of water and the presence of optically dynamic elements, remote sensing offers enormous potential for water-quality monitoring, particularly in Jordan, which has a high number of water-vulnerable bodies.

Water remote detection relies on immediate watercolor perception rather than water tests. It quantifies the relationship between watercolor and ingredients interacting with solar-powered radiation to alter the energy range of reflected radiation from water bodies. Optical water-quality parameters are the term used to describe these elements.

CDOM existing has a significant impact on water column optical properties as it interacts with solar radiation; therefore, the CDOM concentration in the surface water can be determined by remote sensing. Using remote sensing to estimate CDOM can reduce testing costs and provide a spatial and temporal quantification of CDOM, which are the main constraints of traditional field-based water quality measurement [19]. Several multispectral satellites have been used to assess the inland water quality each as Landsat series, Modes, and SPOT XS [20-23]. However, those satellites images had limited by temporal and spatial resolutions. The recently launch Sentinel 2 instrument provide an enhancement in temporal resolution with 5 days' revisit period and better spatial resolution with 10 m and 20 m in wavelength range 490-860 nm [24]. These improved satellite parameters open the door for more investigations of Sentinel-2 potential for estimating inland water quality where few previous studies have used it to developed same works in the lakes [25-28].

The purpose of this research is to assess the utilization of multispectral imaging techniques for monitoring colored dissolved organic materials (CDOM). According to recent studies, a high concentration of CDOM would result in an adverse effect on water purity and quality. Therefore, this research will eventually lead to developing a computational model capable of forecasting CDOM concentrations without the need for in situ measurements and remote monitoring of CDOM concentrations across Jordan's inland water bodies.

2. Materials and Methods

2.1 Study area's

Three Jordanian dams have been chosen for investigation in this study (figure 1). The dams were chosen because of their critical role in Jordan's water sector and the importance of their geographic position, and the variance in CDOM concentration in their water.

The first one is King Talal Dam (KTD), one of the essential projects in the water sector in Jordan. The reason behind that is the size of King Talal Dam and its important role in the Jordanian agricultural sector. According to recent studies, King Talal Dam measures 92 meters in height and 330 meters in width. It has a yearly discharge capacity of 86 million cubic meters and a storage capacity of 75 million cubic meters. This dam is situated in the highlands of Jordan's northern region, on the other side of the Zarqa River. Construction on the dam began in 1971 and was finished in 1972. Building the King Talal dam was an excellent idea for Jordan's agricultural development; it helped increase agricultural production in the Jordan Valley [2]. The water quality of the dam has been significantly affected by the discharge of wastewater plants in the dam's artery [29-31].

Second, Jordan's Wadi Al-Arab Dam (WAD) is located north of Jordan and is considered a vital source of water in this area. This massive dam, which was completed in 1987, was designed to contain 20 million cubic meters of water [32]. The reservoir catchment area is 262 Km^2. This dam's primary goal is to irrigate agriculture in Jordan Valley. Wadi AL- Arab dam water slightly comes from precipitation and the king Abdullah Canal which received water from Wadi Arab and the Yarmouk

River. This dam receives about 400 mm of rain each year, with the majority of the precipitation falling between October to May [33].

Finally, there's the Mujib Dam (MD). The MD is in the Wadi al-Arab, located south of Amman, Jordan's capital city. The dam's capacity is estimated to be around 35 million cubic meters. The dam is a composite dam consisting of a roller compacted concrete (RCC) middle section and a clay core rockfill (CCR) section at both abutments. The construction for this dam started in 1999 and was finished in 2004. The average yearly rainfall at the Mujib Dam is around 70 mm. The water quality in the Al Mujib dam received slightly higher quality than the other Jordanian dam. Therefore, the Mujib dam is mainly used for drinking water and irrigation. In the lower basin, the average temperature is 40°C in summer and 15°C in winter, whereas in the upper basin, the average temperature is 35°C in summer and 10 °C in winter [34].

2.2 Water Sampling and analysis

Ground-based sampling was taken on July 15th, 2019 from KTD, June 30th, 2019 from MD and June 25th, 2019 from WAD. Sixty water samples were taken fairly from these three dams for the purpose of the experiment. Water samples were collected 20 cm below the water's surface and placed in cleaned bottles before being submitted to Petra University lab for analysis. The samples' location was acquired using Global Positioning System (GPS) device. The sampling points' distribution of each dam is shown in figure 1. In the laboratory, CDOM was determined using a spectrophotometer with Mili-Q water as baseline correction [35].

2.3 Sentinel 2 optical sensor and images processing

The Sentinel 2 multispectral instrument (MSI), with 290 km swath width and 12-bit radiometric resolution, has thirteen spectral bands ranging from 430 nm to 2320 nm in the visible (B1-B4), red-edge (B5-B7), near-infrared (B8 and B8a) and shortwave infrared (B9-B12) spectrum region (Table 1). The Sentinel 2 contains two identical satellites, Sentinel-2A and Sentinel-2B, that were launched in 2015 and 2017, respectively. These twin polar-orbiting satellites are running in the sun-synchronous orbit and phased at 180; this provides a high temporal resolution (5 days' revisit time) with two satellites at the equator. Also, the sentinel-2 has relatively high spatial resolutions; three bands with 60 m, six bands with 20 m and four bands with 10 m. Moreover, the MSI sensor improves spectral abilities that comprise beneficial bands for land observations, such as the red-edge bands for water and vegetation studies.

The MSI pictures were taken on the same day as the field sample to avoid any time gap between the in-site measurement and the satellite, which could alter the results. Three data cloud-free images were obtained from the Sentinels Scientific Data Hub (table 2). The Sentinel 2 Level 1-1C (L1C) data contained scaled top of atmosphere reflectance data that resampled to 20 m pixel size using the Sentinel Application Platform (SNAP) version 8.0. Atmospheric conditions significantly affect satellite data and lead to inaccurate using of reflectance data if it is inappropriately corrected. Therefore, the current study was used atmospheric and topographic correction (ATCOR), which perceived as one of the most accurate atmospheric correction methods and is widely used in water applications [36].

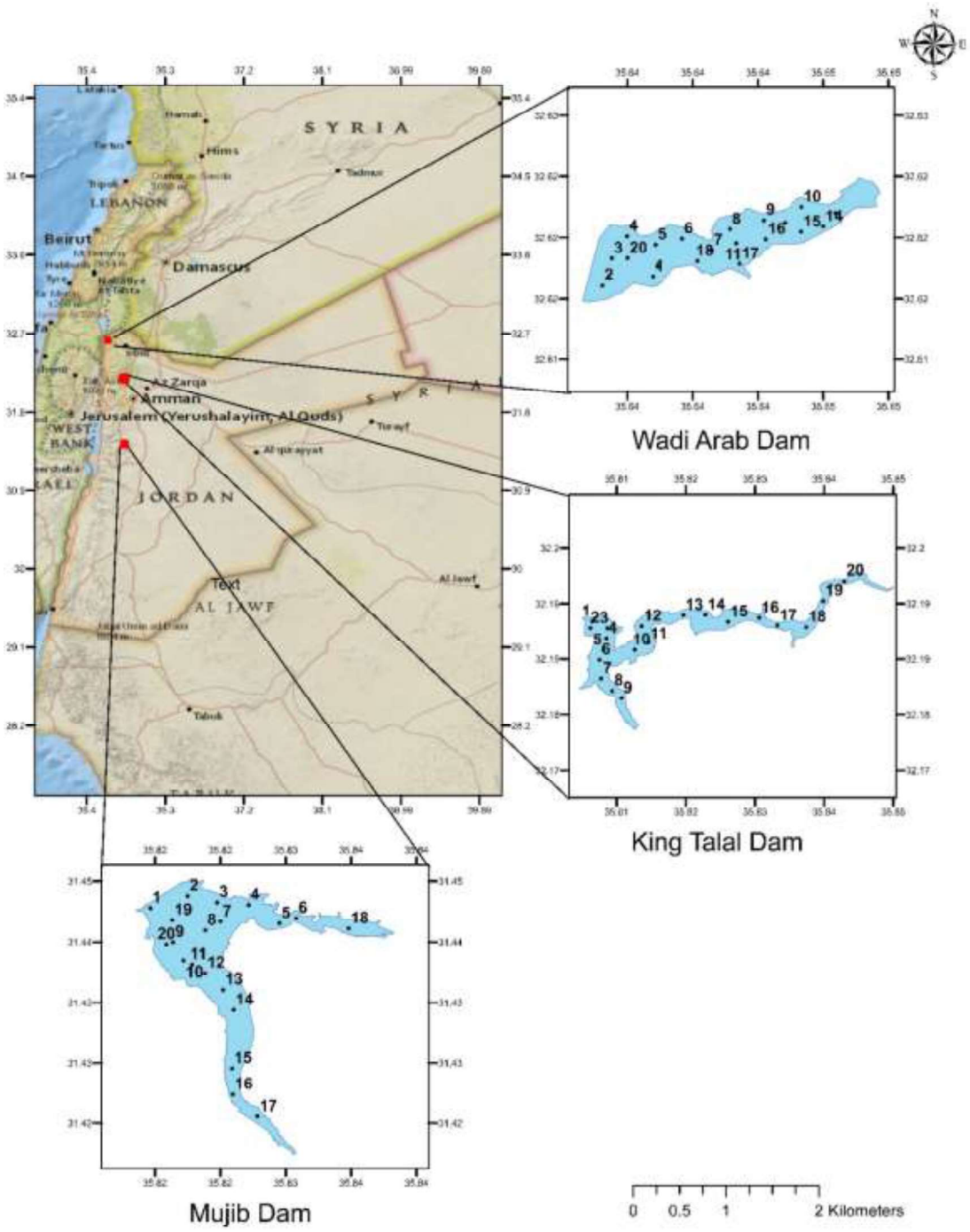

Figure 1: Study areas and sample location points

Table (1): Spectral bands and spatial resolution of Sentinel-2A and Sentinel-2B MSI

Band Number	Spectral Range	Resolution (m)	Bandwidth (nm)	S2A Central wavelength (nm)	S2B Central wavelength (nm)
B1	coastal/aerosol	60	20	442.7	442.2
B2	blue	10	65	492.4	492.1
B3	green	10	35	559.8	559.0
B4	red	10	30	664.6	664.9
B5	VRE	20	15	704.1	703.8
B6	VRE	20	15	740.5	739.1
B7	VRE	20	20	782.8	779.7
B8	NIR	10	115	832.8	832.9
B8a	NIR	20	20	864.7	864.0
B9	WV	60	20	945.1	943.2
B10	cirrus	60	30	1373.5	1376.9
B11	SWIR	20	90	1613.7	1610.4
B12	SWIR	20	180	2202.4	2185.7

Table (2): Sentinel 2 images used in this research

Location	In situ visiting date	Identifier	Sentinel 2 image date	Cloud cover
KTD	2019-07-15	S2B_MSIL1C_20190715T081609_N0208_R121_T36SYA_20190715T120216	2019-07-15	1.41
Mujeeb	2019-06-30	S2A_MSIL1C_20190630T081611_N0207_R121_T36RYV_20190630T102130	2019-06-30	1.36
Wadi Al Arab	2019-06-25	S2B_MSIL1C_20190625T081609_N0207_R121_T36SYB_20190625T120443	2019-06-25	0.00

2.4 Model calibration and validation

To develop the best fit CDOM retrieval model, we tested the linear, exponential, power and logarithmic for a single band and several combinations of two-band ratio models. The 60 samples were randomly divided into 40 samples for calibration and the rest (20 samples) for validation. The coefficient of determination (R^2) was used to evaluate the goodness of fit of the calibrated model. Then, the accuracy of the predicted models was compred using four statistical indicators: coefficient of determination (R^2), root-mean-squared error (RMSE), Mean Absolute Error (MAE), and bias.

$$\text{RMSE}= \sqrt{\frac{1}{N}\sum_{i=1}^{n}[xi^{predicted} - xi^{measured}]^2} \quad (1)$$

$$\text{MAE}=\frac{\sum_{i=1}^{n}|xi^{predicted}-xi^{measured}|}{N} \quad (2)$$

$$\text{Bias}=\frac{\sum_{i=1}^{n}[xi^{predicted}-xi^{measured}]}{N} \quad (3)$$

Where $xi^{predicted}$ and $xi^{measured}$ represent respectively the predicted and measured CDOM concentration, N is the number of samples.

3. Results and Discussion

3.1 Observed CDOM data

The measured CDOM concentrations of samples obtained from the three selected dams and the locations of sampling points are shown in figure (2-4). According to lab data, KTD has the highest average CDOM concentration, which reflected the effect of treated wastewater discharge to the dam and explaining why KTD can only be utilized for agriculture purposes. The Average CDOM concentration reached 12.77 m^{-1}, which is relatively higher than the other two dams. According to the statistics shows in table 3, the WAD came second for an average of 7.32 m^{-1} CDOM concentrations. That means that WAD water is not safe to be used as drinking water for humans or animals. Therefore, for this case, Wadi Al -Arab also can only be utilized for agriculture purposes.

From the statistics table (3), we can readily see that CDOM concentration is slightly low in the MD CDOM concentrate average. The CDOM concentration was only 2.84 m^{-1} on average at the time. Therefore, the MD may be the only one used for safe drinking water between these three dams. In this scenario, the Jordanian government is working hard to ensure that this dam is secure and free of any contaminants that could threaten AL-Mujib dam water quality.

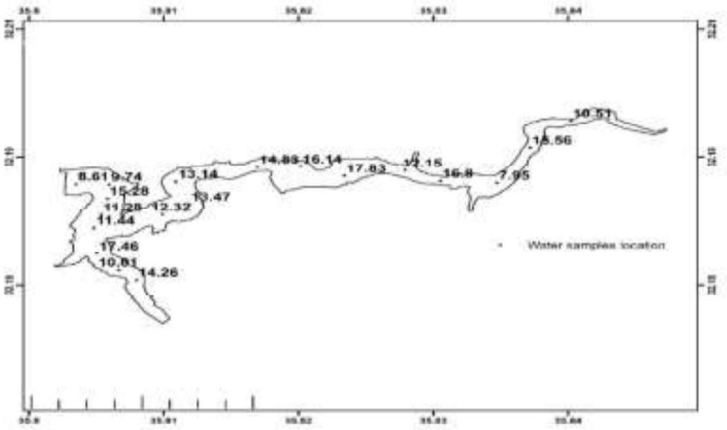

Figure (2): Distribution of king Talal dam sampling locations.

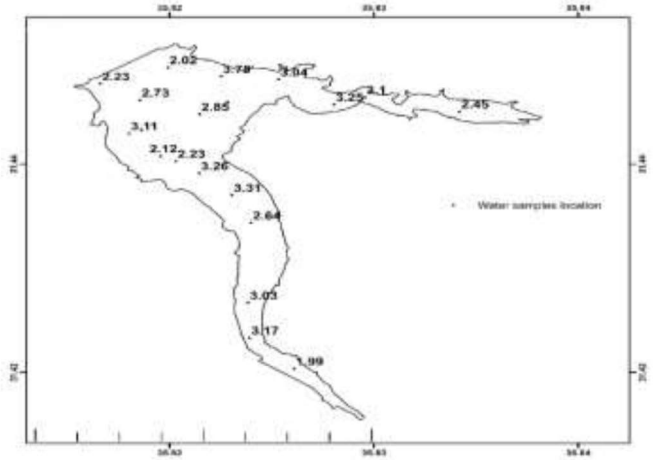

Figure (3): Distribution of Mujib dam sampling locations.

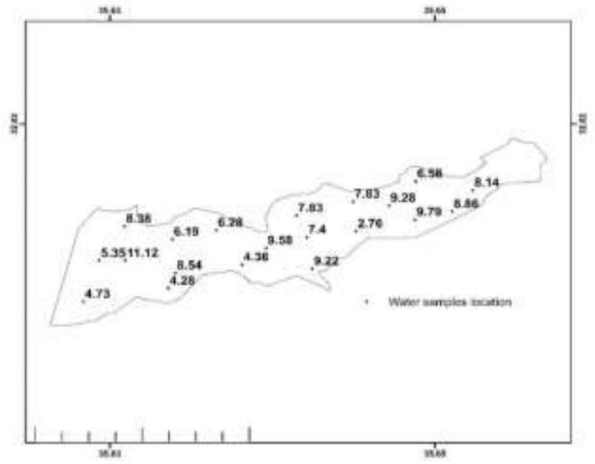

Figure (4): Distribution of Wadi Al-Arab dam sampling locations**.**

Table (3): CDOM descriptive statistics in three dams

	KTD				**MD**				**WAD**			
Statistics	Min	Max	Ave	SD	Min	Max	Ave	SD	Min	Max	Ave	SD
CDOM m^{-1}	7.32	17.83	12.77	3.19	1.99	3.83	2.84	0.54	2.76	11	7.32	2.18

3.2 Colored Dissolved Organic Matter Retrieval model

In this research, 60 water samples were collected between the three dams (King Talal Dam, Mujib Dam, and Wadi Al-Arab Dam) and considered for investigation. The collected data were divided into two sets. The first set contained 40 points and was used for calibration. The second set contained 20 points and was used for validation. The CDOM algorithms applied to the Sentinel 2 spectral band configuration in the literature use ratios and combinations of two and single bands.

3.2.1 Calibration of regression models

The exponential and power relationship was observed in all band combinations between the tested blue and green Sentinel-2 bands and CDOM. This research detected that the relationship between Sentinel-2 reflectance and blue to green bands ratio was preferred to other combinations. Figures 5-7 presented the best-founded calibrated regression between the CDOM and the Sentinel-2 reflectance.

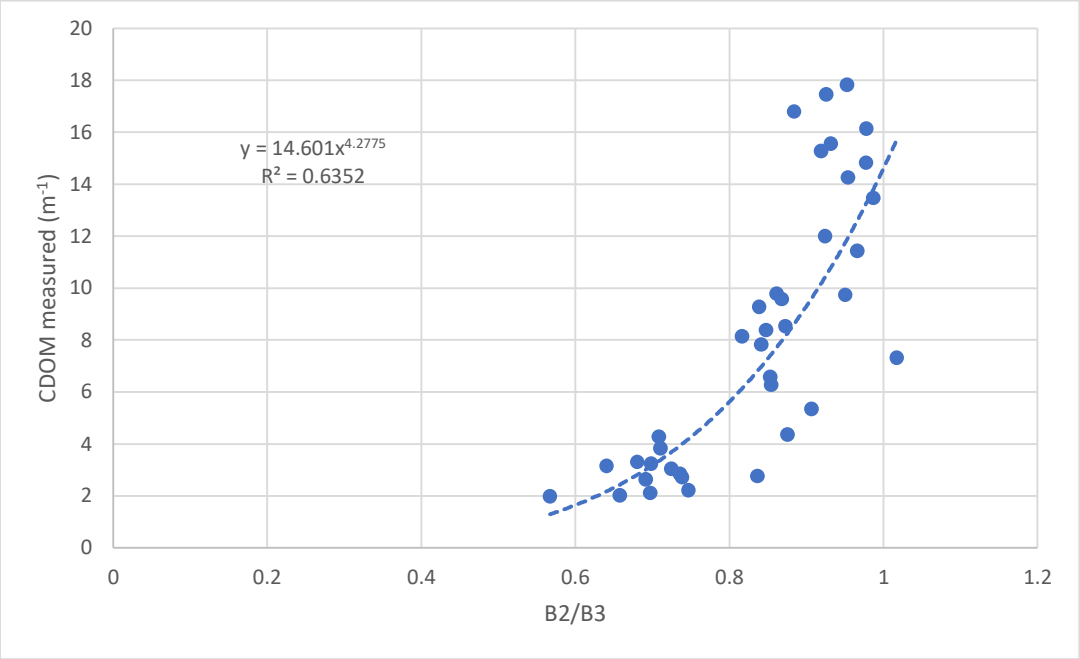

Figure 5: Regression between the Sentinel 2 band index and measured CDOM, using the B2/B3 model

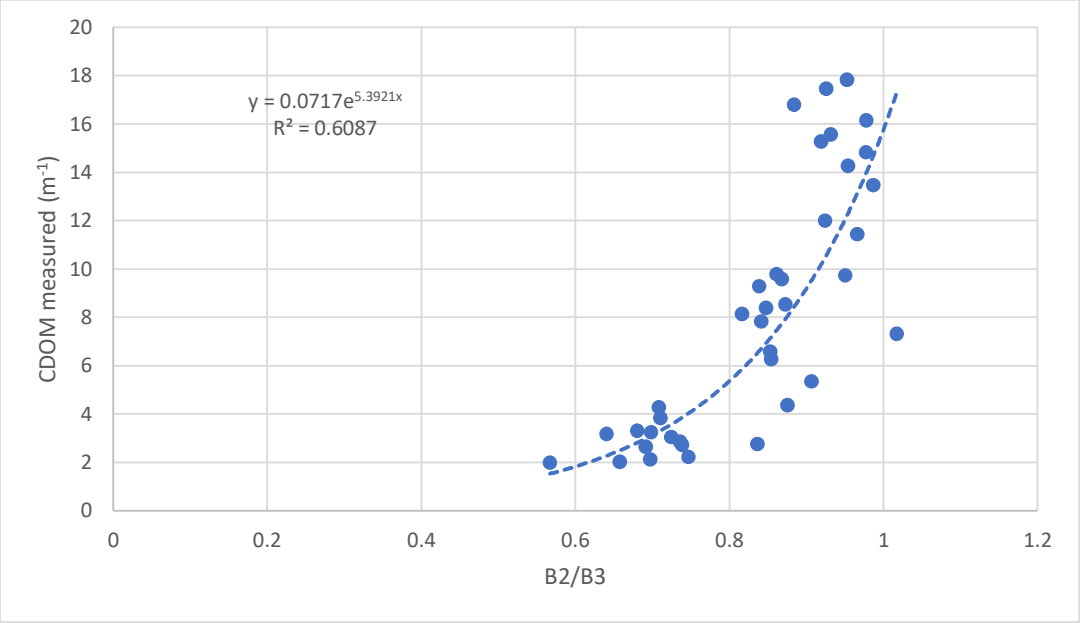

Figure 6: Regression between the Sentinel 2 band index and measured CDOM, using the B2/B3 model

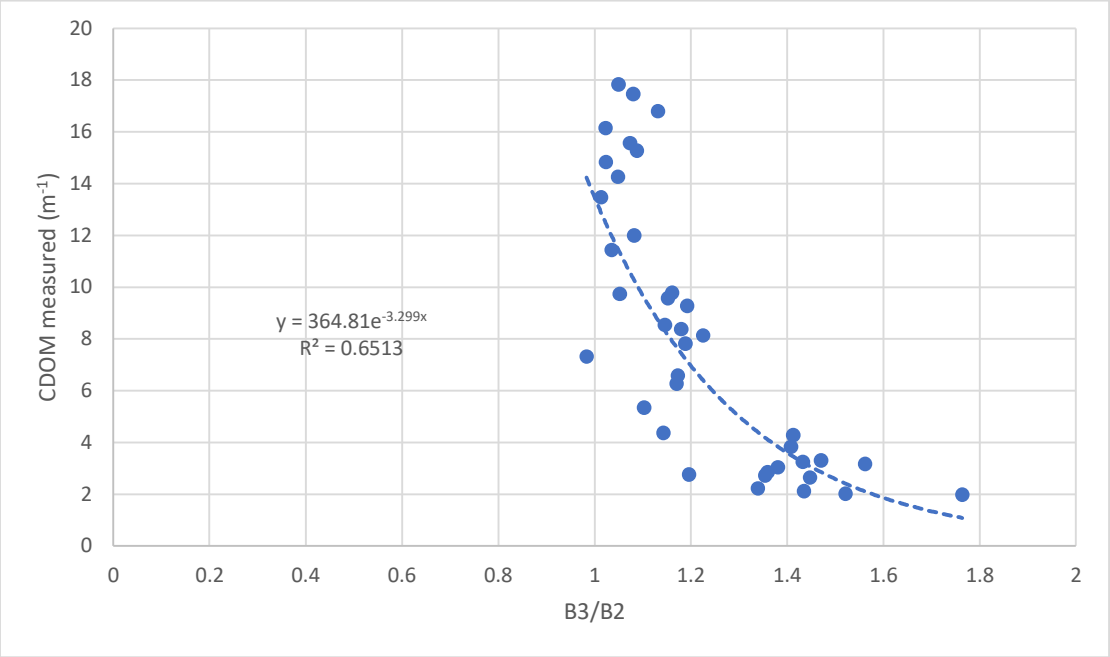

Figure 7: Regression between the Sentinel 2 band index and measured CDOM using the B2/B3 model

3.2.2 validation of regression models

In this study, regression analysis was used to develop the relation between CDOM and Setinal 2 data on the study areas. The calibration results show that three developed models were providing a suitable fitting as shown in Figure 5-7. These models were then validated using a dataset that has never been used for the calibration. The scatter plot of the measured versus predicted is shown in Figure 8-10.

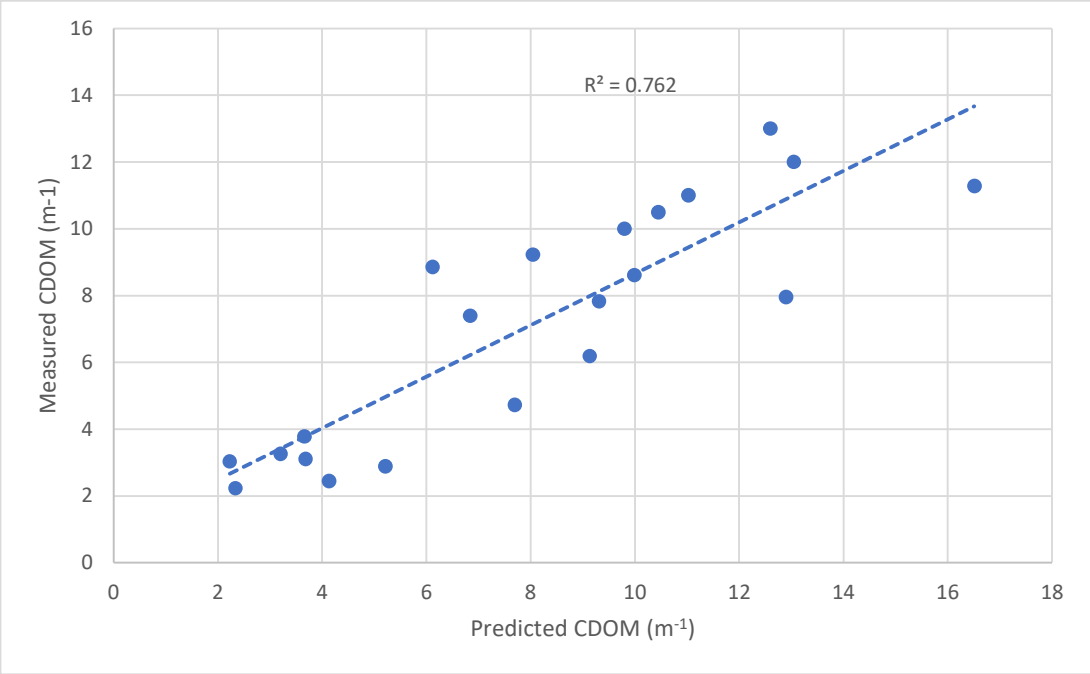

Figure 8: Regression between predicted and measured CDOM using the B2/B3 power model.

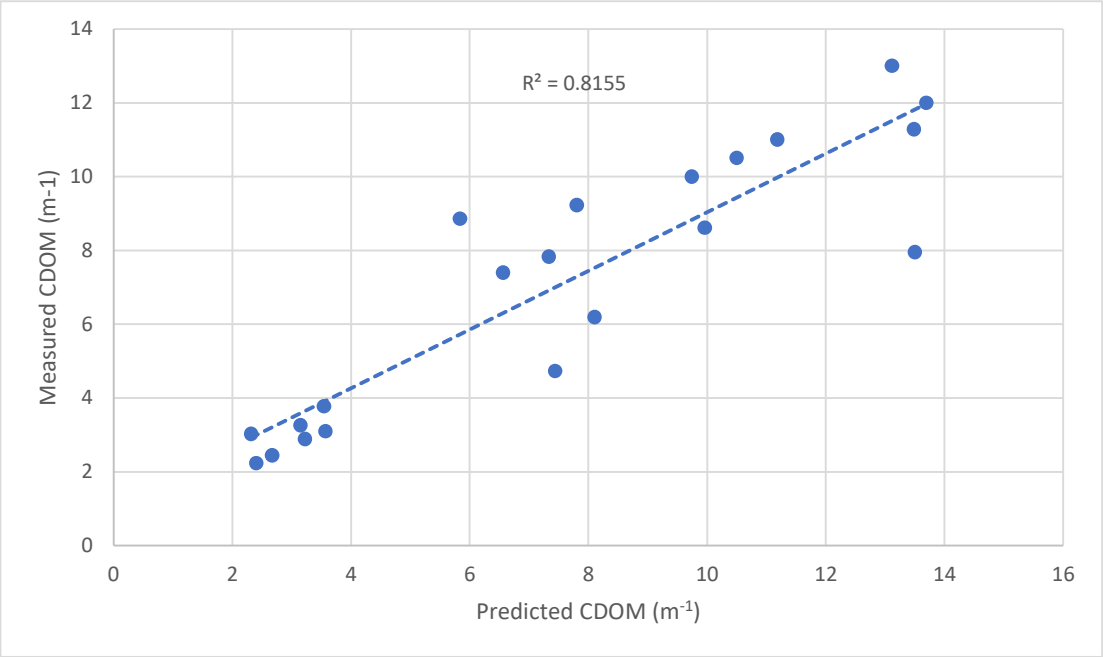

Figure 9: Regression between predicted and measured CDOM using the B2/B3 exponential model.

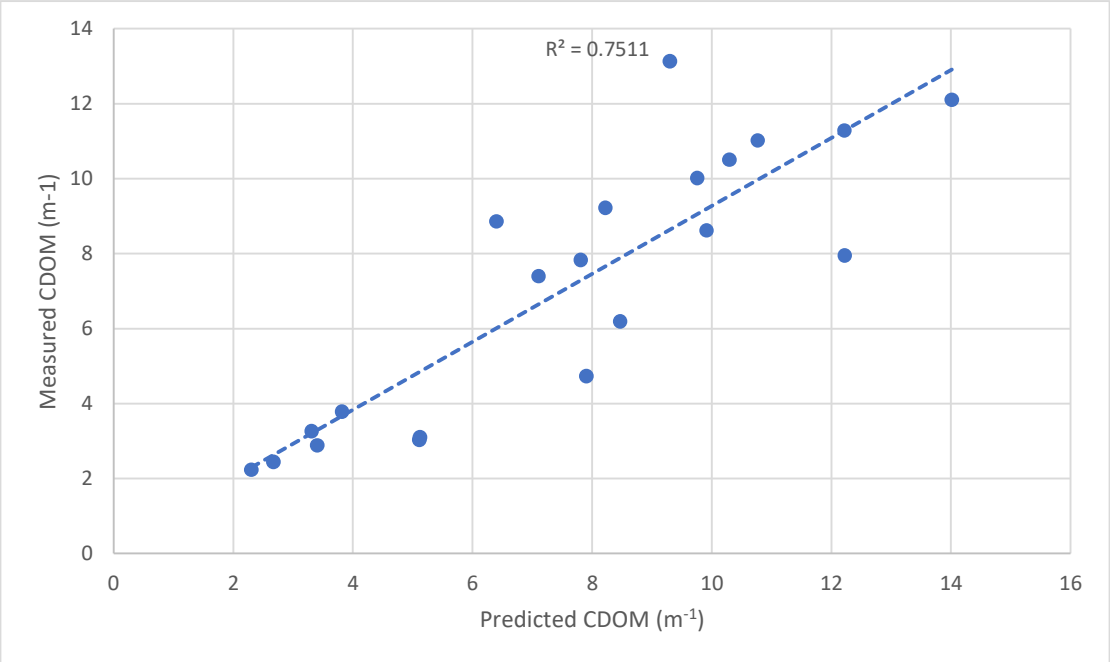

Figure 10: Regression between predicted and measured CDOM using the B2/B3 exponential model.

The estimation errors of a blue to green exponential model (B2/B3) were provided the best fitting regression with a RMSE of 1.754 m^{-1}, a MAE of 1.144 m^{-1} and a Bias of -0.469 m^{-1} (Table 4).

Table 4: Validation results of Sentinel 2 CDOM models.

Index	Equation	R^2	RMSE	MAE	Bias
B2/B3	y = 14.601x4.2775	0.762	2.014	1.406	-0.825
B2/B3	y = 0.0717e5.3921x	0.815	1.754	1.144	-0.469
B3/B2	y = 364.81e-3.299x	0.752	1.842	1.295	-0.491

3.3 Mapping CDOM constriction using the Sentinel 2 Retrieval model

The best-fitting model of sentinel-2 (exponential function of B2/B3) was used to produce spatial distribution maps of the CDOM (m^{-1}) inside the three studied dams; KTD (Figure 11), MD (Figure 12) and WAD (Figure 13). The outputs indicate that the Sentinel-2 retrieval model can generate reasonable accurate maps of CDOM in varying concentration levels.

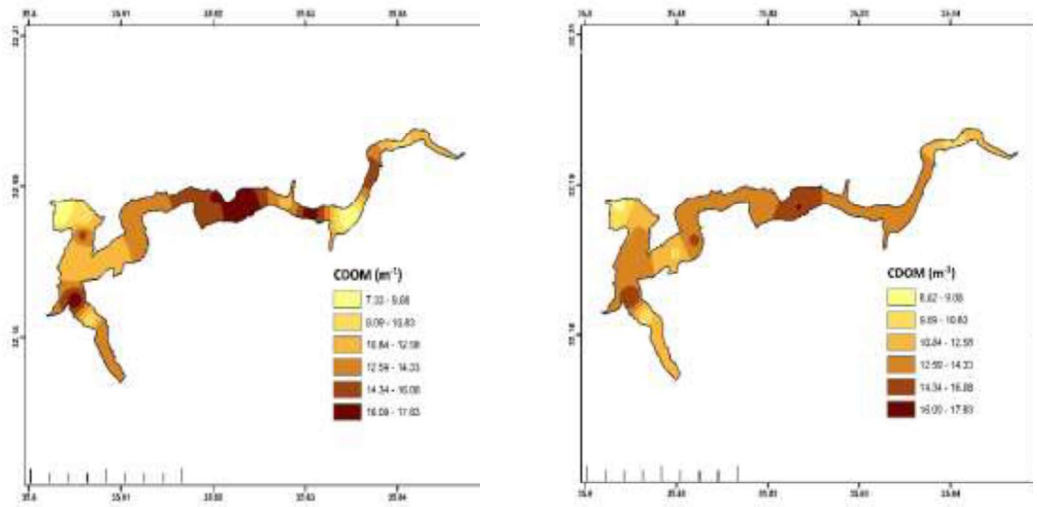

(a) (b)

Figure 11: CDOM distribution on KTD estimated from (a) laboratory analysis and (b) Sentinel-2

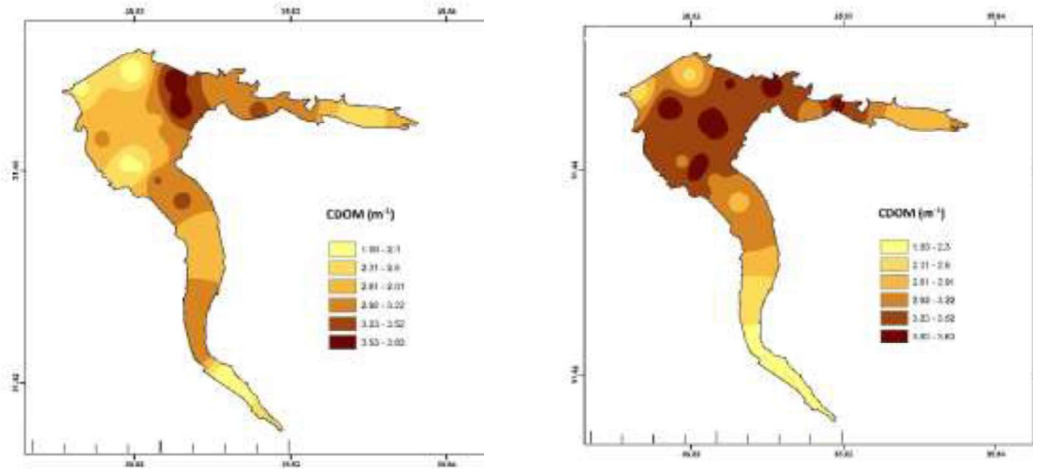

(a) (b)

Figure 12: CDOM distribution on MD estimated from (a) laboratory analysis and (b) Sentinel-2

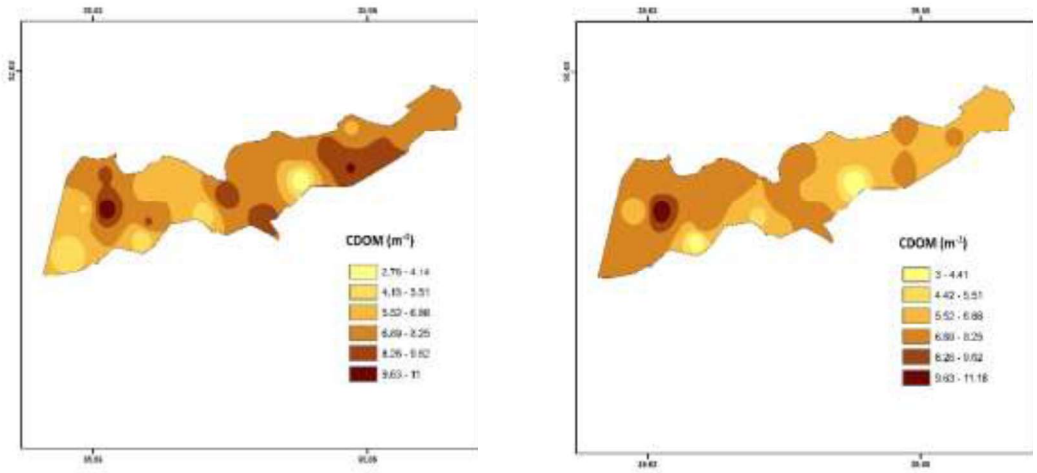

(a) **(b)**

Figure 13: CDOM distribution on WAD estimated from (a) laboratory analysis and (b) Sentinel-2.

4. Conclusions

The applicability and accuracy of using sentinel 2 images to evaluate and monitor CDOM concentration in inland water bodies were evaluated in this investigation. Three diverse Jordanian's dams were picked for CDOM concentration test. Regarding this regard, 60 samples were collected relatively and were measured. According to output results, it appears that three Jordanian dams have different water-quality properties and significant variations in CDOM concentration levels. The statistics results show that CDOM concentration in KTD was the highest between the three dams.

The CDOM concentration in KTD has reached 12.77 m^{-1} on average. However, the MD gets the lowest CDOM concentration, making it the safest dam regarding drinking water. The CDOM concentration of MD was approximately 2.84 m^{-1}on average. Lastly, Wadi Al Arab dam has taken second place as CDOM concentration Level. The average concentration of that dam reached 7.32 m^{-1}.

The empirical model approach was applied to create a CDOM predictive model by testing and examining several bands-based algorithms. A predictive model was developed using about two-thirds of the samples. The created model was used to forecast CDOM concentrations using surface reflectance data for the remaining 20 sampling stations. The validation set's measured CDOM concentrations were compared to the matching anticipated values derived from established models. The exponential of the blue to green ratio model demonstrated the highest capabilities to retrieve CDOM concentration with RMSE of 1.754 m^{-1}, MAE of 1.144 m^{-1} and Bias of -0.469 m^{-1}.

Acknowledgments: authors would like to thank the Deanship of Scientific Research and Graduate Studies at University of Petra (grant no. 3/7/2019).

References

1. Odeh, T.; Mohammad, A. H., Wise Water Resources Management under the Increasing Number of Refugees in the Third Poorest Water Resources Country (Jordan)–A Suggested Future Spatial Plan for Water Resources Investments. International Journal of Sustainable Development and Planning 2020, 15, (2), 235-238.
2. Hadadin, N., Dams in Jordan current and future perspective. Canadian journal of pure applied sciences 2015, 9, (1), 3279-3290.
3. Hammouri, N.; Adamowski, J.; Freiwan, M.; Prasher, S., Climate change impacts on surface water resources in arid and semi-arid regions: a case study in northern Jordan. Acta Geodaetica et Geophysica 2017, 52, (1), 141-156.
4. Odeh, T.; Boulad, N.; Abed, O.; Abu Yahya, A.; Khries, N.; Abu-Jaber, N., The influence of Geology on landscape typology in Jordan: theoretical understanding and planning implications. Land 2017, 6, (3), 51.
5. WATER MANAGEMENT INITIATIVE Review of Water Scarcity Ranking Methodologies; United States Agency for International Development Amma, Jordan, 2017.
6. Tranvik, L. J., Carbon cycling in the Arctic. Science 2014, 345, (6199), 870-870.
7. Battin, T. J.; Luyssaert, S.; Kaplan, L. A.; Aufdenkampe, A. K.; Richter, A.; Tranvik, L. J., The boundless carbon cycle. Nature Geoscience 2009, 2, (9), 598-600.
8. Stedmon, C. A.; Markager, S.; Kaas, H., Optical properties and signatures of chromophoric dissolved organic matter (CDOM) in Danish coastal waters. Estuarine, Coastal Shelf Science 2000, 51, (2), 267-278.
9. Parry, M.; Parry, M. L.; Canziani, O.; Palutikof, J.; Van der Linden, P.; Hanson, C., Climate change 2007-impacts, adaptation and vulnerability: Working group II contribution to the fourth assessment report of the IPCC. Cambridge University Press: 2007; Vol. 4.
10. Kutser, T.; Hedley, J.; Giardino, C.; Roelfsema, C.; Brando, V. E., Remote sensing of shallow waters–A 50 year retrospective and future directions. Remote Sensing of Environment 2020, 240, 111619.
11. Li, J.; Yu, Q.; Tian, Y. Q.; Becker, B. L., Remote sensing estimation of colored dissolved organic matter (CDOM) in optically shallow waters. ISPRS Journal of Photogrammetry Remote Sensing 2017, 128, 98-110.
12. Dvornikov, Y.; Leibman, M.; Heim, B.; Bartsch, A.; Herzschuh, U.; Skorospekhova, T.; Fedorova, I.; Khomutov, A.; Widhalm, B.; Gubarkov, A., Terrestrial CDOM in lakes of Yamal peninsula: connection to lake and lake catchment properties. Remote Sensing 2018, 10, (2), 167.
13. Al-Kharusi, E. S.; Tenenbaum, D. E.; Abdi, A. M.; Kutser, T.; Karlsson, J.; Bergström, A.-K.; Berggren, M., Large-scale retrieval of coloured dissolved organic matter in northern lakes using Sentinel-2 data. Remote Sensing 2020, 12, (1), 157.
14. Liu, D.; Yu, S.; Xiao, Q.; Qi, T.; Duan, H., Satellite estimation of dissolved organic carbon in eutrophic Lake Taihu, China. Remote Sensing of Environment 2021, 264, 112572.
15. Markager, S.; Vincent, W. F., Spectral light attenuation and the absorption of UV and blue light in natural waters. Limnology Oceanography 2000, 45, (3), 642-650.

16. Hestir, E. L.; Brando, V.; Campbell, G.; Dekker, A.; Malthus, T., The relationship between dissolved organic matter absorption and dissolved organic carbon in reservoirs along a temperate to tropical gradient. Remote Sensing of Environment 2015, 156, 395-402.
17. Del Vecchio, R.; Blough, N. V., Spatial and seasonal distribution of chromophoric dissolved organic matter and dissolved organic carbon in the Middle Atlantic Bight. Mar. Chem. 2004, 89, (1-4), 169-187.
18. Pielke Sr, R. A., Mesoscale Modeling and Satellite Simulator. In International Geophysics, Elsevier: 2013; Vol. 98, pp 407-426.
19. Torbick, N.; Hu, F.; Zhang, J.; Qi, J.; Zhang, H.; Becker, B., Mapping chlorophyll-a concentrations in West Lake, China using Landsat 7 ETM+. Journal of Great Lakes Research 2008, 34, (3), 559-565.
20. Womber, Z. R.; Zimale, F. A.; Kebedew, M. G.; Asers, B. W.; DeLuca, N. M.; Guzman, C. D.; Tilahun, S. A.; Zaitchik, B. F., Estimation of Suspended Sediment Concentration from Remote Sensing and In Situ Measurement over Lake Tana, Ethiopia. Advances in Civil Engineering 2021, 2021.
21. He, Y.; Jin, S.; Shang, W., Water quality variability and related factors along the Yangtze River using Landsat-8. Remote Sensing 2021, 13, (12), 2241.
22. Zhu, W.; Huang, L.; Sun, N.; Chen, J.; Pang, S., Landsat 8-observed water quality and its coupled environmental factors for urban scenery lakes: A case study of West Lake. Water Environ. Res 2020, 92, (2), 255-265.
23. Hu, M.; Ma, R.; Cao, Z.; Xiong, J.; Xue, K., Remote Estimation of Trophic State Index for Inland Waters Using Landsat-8 OLI Imagery. Remote Sensing 2021, 13, (10), 1988.
24. Hedley, J.; Roelfsema, C.; Koetz, B.; Phinn, S., Capability of the Sentinel 2 mission for tropical coral reef mapping and coral bleaching detection. Remote Sensing of Environment 2012, 120, 145-155.
25. Hussein, N. M.; Assaf, M. N., Multispectral Remote Sensing Utilization for Monitoring Chlorophyll-a Levels in Inland Water Bodies in Jordan. The Scientific World Journal 2020, 2020.
26. Assaf, M. N. Utilizing Landsat 8 and Sentinel 2 Satellites Images for Water Quality Evaluation in King Tala Dam. German Jordanian University, 2019.
27. Chen, J.; Zhu, W.; Tian, Y. Q.; Yu, Q.; Zheng, Y.; Huang, L., Remote estimation of colored dissolved organic matter and chlorophyll-a in Lake Huron using Sentinel-2 measurements. Journal of Applied Remote Sensing 2017, 11, (3), 036007.
28. Ouma, Y. O.; Noor, K.; Herbert, K., Modelling Reservoir Chlorophyll-a, TSS, and Turbidity Using Sentinel-2A MSI and Landsat-8 OLI Satellite Sensors with Empirical Multivariate Regression. Journal of Sensors 2020, 2020.
29. Hilal, A. H. A.; Alhaija, M. M. A., Nutrients in Water and Sediments of King Talal Dam-Jordan. Jordan Journal of Biological Sciences 2010, 3, (3), 87-100.
30. Abualhaija, M. M.; Shammout, M. a. W.; Mohammad, A.-H.; Hilal, A. H. A., Heavy Metals in water and sediments of King talal Dam the largest Man-Made water Body in Jordan. Water Energy International 2019, 62, (5), 49-62.
31. Al-Taani, A. A.; El-Radaideh, N. M.; Al Khateeb, W. M., Status of water quality in King Talal Reservoir Dam, Jordan. Water Resources 2018, 45, (4), 603-614.
32. Shatnawi, A.; Diabat, A., Siltation of Wadi Al-Arab reservoir using GIS techniques. Jordan Journal of Civil Engineering 2016, 10, (4).
33. Saadoun, I.; Batayneh, E.; Alhandal, A.; Hindieh, M., Physicochemical features of Wadi Al-Arab Dam (reservoir), Jordan. Oceanological Hydrobiological Studies 2010, 39, (4), 189-203.
34. Yusra, A.-h., Landforms Classification of Wadi Al-Mujib Basin in Jordan, based on Topographic Position Index (TPI), and the production of a flood forecasting map. Dirasat, Human Social Sciences 2019, 46, (3).
35. Zhu, W.; Yu, Q.; Tian, Y. Q.; Becker, B. L.; Zheng, T.; Carrick, H. J., An assessment of remote sensing algorithms for colored dissolved organic matter in complex freshwater environments. Remote Sensing of Environment 2014, 140, 766-778.

36. Bilal, M.; Nazeer, M.; Nichol, J. E.; Bleiweiss, M. P.; Qiu, Z.; Jäkel, E.; Campbell, J. R.; Atique, L.; Huang, X.; Lolli, S., A Simplified and Robust Surface Reflectance Estimation Method (SREM) for Use over Diverse Land Surfaces Using Multi-Sensor Data. Remote Sensing 2019, 11, (11), 1344.